Use of Second-Order Switching Surface in the Boundary Control of Buck Converter

Kelvin K.S. Leung and Henry S.H. Chung†

Department of Electronic Engineering
City University of Hong Kong
Tat Chee Avenue, Kowloon Tong, Kowloon, Hong Kong SAR, China
†Fax.: (852) 2788 7791
†Email: eeshc@cityu.edu.hk

Abstract - **A second-order switching surface in the boundary control of buck converters is studied in this paper. The formulated switching surface can make the overall converter exhibit better steady-state and transient behaviors than the one with first-order switching surface. Most importantly, it is applicable for converters operating in both continuous and discontinuous conduction modes. The switching surface is derived from estimating the state trajectory movement after a switching action, resulting in a high state trajectory velocity along the switching surface. This phenomenon accelerates the trajectory moving towards the target operating point. The proposed control scheme has been successfully applied to a 120W buck converter. Detailed large-signal characteristics and comparisons with the first-order switching surface will be discussed.**

Index Terms - Boundary control, dc-dc conversion, large-signal stability

I. INTRODUCTION

Switching converters are an important class of systems that operate by variable structure control. Boundary control is a geometric based control method suitable for those switching converters having time-varying circuit topology. Based on the large-signal trajectories of the converter on the state plane, a switching surface is defined to dictate the switching actions. An ideal switching surface can achieve global stability, good large-signal operation, and fast dynamics [1]. Detailed investigations into the modeling, design, and analysis of the boundary control with first-order switching surface are studied in [1]-[3].

Among various boundary control methods with first-order switching surfaces, sliding-mode control and hysteresis control are widely used in power converters [4]-[7]. Although all those methods generally provide good large-signal performance and stability, the transient dynamics is not optimized. Much research work extend those concepts, such as the adaptive-hysteresis control in [8, 9], to enhance the dynamics. However, many of them are only applicable for dc/dc converters operating in continuous conduction mode. When a converter is operated in the discontinuous conduction mode, an additional boundary due to the zero inductor current is created inherently. An unstable combination may be emerged [2]. Moreover, with the presence of hysteresis band, the output will even have steady-state error.

A second-order switching surface in the boundary control of buck converters is presented in this paper. The proposed switching surface enhances the tangential velocity of the trajectories along the switching surface, so that the converter exhibit better transient behaviors than the one with the first-order switching surface. Instead of guiding the state trajectory movement as in the first-order switching surface, the proposed surface is derived from the natural movement of the state trajectory after a switching action. The scheme is applicable for converters operating in both continuous and discontinuous conduction modes. The proposed control scheme has been successfully applied to a 120W buck converter.

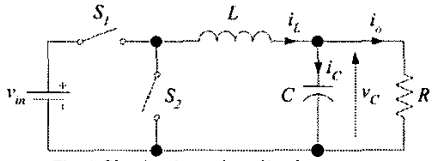

Fig. 1 Circuit schematics of buck converter.

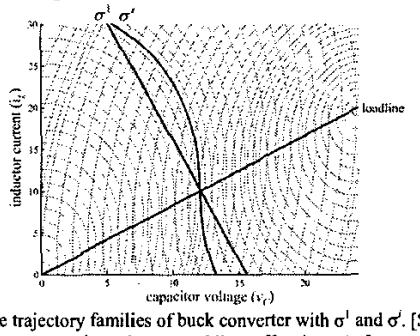

Fig. 2 State trajectory families of buck converter with σ^1 and σ^2. [Solid line: on-trajectories, Dotted line: off-trajectories]

II. FIRST- AND SECOND-ORDER SWITCHING SURFACES

The buck converter shown in Fig. 1 can be expressed by the state-space equation of

$$\dot{x} = A_0 x + B_0 u + (A_1 x + B_1 u) q_1 + (A_2 x + B_2 u) q_2 \quad (1)$$

where $x = [i_L \quad v_C]$, A_i and B_i are constant matrix and q_i represents the state of the switch S_i. S_i is on if $q_i = 1$, and is off if $q_i = 0$. Matrices A_0, B_0, A_1, B_1, A_2, and B_2 are defined as $A_0 = \begin{bmatrix} 0 & 0 \\ 0 & -\frac{1}{RC} \end{bmatrix}$, $B_0 = \begin{bmatrix} 0 \\ 0 \end{bmatrix}$, $A_1 = \begin{bmatrix} 0 & -\frac{1}{L} \\ \frac{1}{C} & 0 \end{bmatrix}$, $B_1 = \begin{bmatrix} \frac{1}{L} \\ 0 \end{bmatrix}$, $A_2 = \begin{bmatrix} 0 & -\frac{1}{L} \\ \frac{1}{C} & 0 \end{bmatrix}$, and $B_2 = \begin{bmatrix} 0 \\ 0 \end{bmatrix}$.

A family of the on- and off-state trajectories, as well as the load line, is shown in Fig. 2. They are obtained by solving (1) with different initial conditions. The component values used in the analysis are tabulated in Table I. The on-state trajectory is obtained by setting $\{q_1, q_2\} = \{1, 0\}$, while the off-state trajectory is obtained by setting $\{q_1, q_2\} = \{0, 1\}$. As discussed in [1], the tangential component of the state-trajectory velocity on the switching surface determines the rate at which successor

points approach or recede from the target operating point. An ideal switching surface σ^i that gives fast dynamics should be on the only trajectory passing through the target operating point. Once the converter state reaches the surface, it will theoretically attract to the target operating point in one successive switching cycle. As shown in Fig. 2, the surface of σ^i above the load line should be along the only off-state trajectory that passes the target operating point and the surface of σ^i below the load line should be along the only on-state trajectory that passes the target operating point. The converter will follow the off-state trajectory, when its state is at the right hand side of σ^i. The converter will follow the on-state trajectory, when its state is at the left hand side of σ^i.

A typical first-order switching surface σ^1 is shown in Fig. 2. It can be written in the following form with one reference setting

$$\begin{aligned}\sigma^1(i_L, v_C) &= c_1 i_C + (v_C - v_{ref}) \\ &= c_1 (i_L - \frac{v_C}{R}) + (v_C - v_{ref})\end{aligned} \quad (2)$$

where i_C and v_C are the capacitor current and voltage, respectively, i_L is the inductor current, c_1 is the gain, R is the load resistance, and v_{ref} is the desired output voltage.

Thus, the tangential state-trajectory velocity on σ^1 is non-optimal that the transient dynamics may take several switching cycles. A second-order surface σ^2, which is near to the ideal surface around the operating point, is derived in the following. The concept is based on estimating the state trajectory after a hypothesized switching action. If the output ripple voltage is much smaller than the average output voltage at the steady state, the output current i_o is relatively constant. Since $i_L = i_C + i_o$, the change of i_L, Δi_L, equals the change of i_C, Δi_C. Fig. 3 shows the typical waveforms of v_C and i_C. v_C varies between a maximum value of $v_{C,\max}$ and a minimum value of $v_{C,\min}$. The state of S is determined by predicting the area under i_C with a hypothesized switching action till $i_C = 0$ and comparing the area with a fixed ratio of the output error at that instant. Criteria for switching S_1 are given as below.

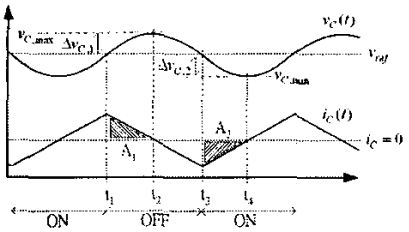

Fig. 3 Typical waveforms of v_C and i_L of buck converter.

1) Criteria for switching off S_1

As depicted in Fig. 3, S_1 is originally in the on state and is switched off at the hypothesized time instant t_1. The objective is to determine t_1, so that v_C is equal to $v_{C,\max}$ at t_2 (at which $i_C = 0$). The shaded area A_1 under i_C is integrated from t_1 to t_2. Thus,

$$\Delta v_{C,1} = v_{C,\max} - v_C(t_1) = \frac{1}{C}\int_{t_1}^{t_2} i_C \, dt \quad (3)$$

A_1 is approximated by a triangle. It can be shown that

$$\int_{t_1}^{t_2} i_C \, dt \cong \frac{1}{2}\frac{L\, i_C^2(t_1)}{v_C(t_1)} \quad (4)$$

In order to ensure that v_C will not go above $v_{C,\max}$, S_1 should be switched off when

$$v_C(t_1) \geq v_{C,\max} - \frac{1}{2}\frac{L\, i_C^2(t_1)}{C\, v_C(t_1)} = v_{C,\max} - k_1(v_C)\, i_C^2(t_1) \quad (5)$$

and

$$i_C(t_1) > 0 \quad (6)$$

2) Criteria for switching on S_1

As depicted in Fig. 3, S_1 is originally off and is switched on at the hypothesized time instant t_3. The objective is to determine t_3, so that v_C is equal to $v_{C,\min}$ at t_4 (at which $i_C = 0$). The shaded area A_2 under i_C is integrated from t_3 to t_4. Thus,

$$\Delta v_{C,2} = v_{C,\min} - v_C(t_3) = \frac{1}{C}\int_{t_3}^{t_4} i_C \, dt \quad (7)$$

Again, if A_2 is approximated by a triangle, it can be shown that

$$\int_{t_3}^{t_4} i_C \, dt \cong -\frac{1}{2}\frac{L\, i_C^2(t_3)}{[v_{in}(t_3) - v_C(t_3)]} \quad (8)$$

In order to ensure that v_C will not go below $v_{C,\min}$, S_1 should be switched on when

$$\begin{aligned} v_C(t_3) &\leq v_{C,\min} + \frac{1}{2}\frac{L i_C^2(t_3)}{C[v_{in}(t_3) - v_C(t_3)]} \\ &= v_{C,\min} + k_2(v_{in}, v_C)\, i_C^2(t_3) \end{aligned} \quad (9)$$

and

$$i_C(t_3) < 0 \quad (10)$$

For simplicity, k_1 and k_2 are obtained by using the nominal values of v_{in} and v_C. Based on (5), (6), (9), (10), and $v_{C,\min} = v_{C,\max} = v_{ref}$, the following σ^2 can be concluded,

$$\sigma^2(i_L, v_C) = \begin{cases} k_1 (i_L - \frac{v_C}{R})^2 + (v_C - v_{ref}), & (i_L - \frac{v_C}{R}) > 0 \\ -k_2 (i_L - \frac{v_C}{R})^2 + (v_C - v_{ref}), & (i_L - \frac{v_C}{R}) < 0 \end{cases} \quad (11)$$

The equation can further be written into a single expression of

$$\sigma^2(i_L, v_C) = c_2 (i_L - \frac{v_C}{R})^2 + (v_C - v_{ref}) \quad (12)$$

where

$$c_2 = \frac{1}{2}k_1\left(1 + \mathrm{sgn}(i_L - \frac{v_C}{R})\right) - \frac{1}{2}k_2\left(1 - \mathrm{sgn}(i_L - \frac{v_C}{R})\right) \text{ and } \mathrm{sgn}(v) = \begin{cases} 1, & v > 0 \\ 0, & v = 0 \\ -1, & v < 0 \end{cases}.$$

Compared (12) with σ^1 in (2), σ^2 consists of a second-order term. σ^2 is close to σ^i near the operating point. However, discrepancies occur, when the state is far from the operating point because of the approximations in

(4) and (8). Implementation of the controller is shown in Fig. 4.

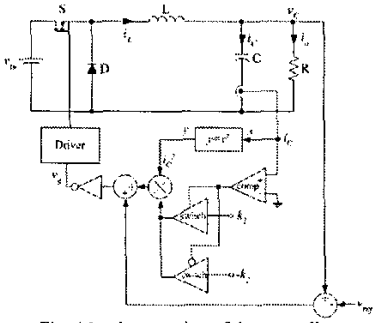

Fig. 4 Implementation of the controller.

III. LARGE-SIGNAL CHARACTERISTICS

Points along $\sigma = 0$ can be classified into refractive, reflective, and rejective modes. The dynamics of the system will exhibit differently in these regions [1]. For σ^2, the transition boundary is obtained by differentiating (12)

$$\frac{d i_L}{d v_C}\Big|_{on,off} = \frac{1}{R} + \frac{1}{2}\frac{i_L - \frac{v_C}{R}}{v_C - v_{ref}} \tag{13}$$

Detailed derivation of (13) can be found in the Appendix.

The expression at the left-hand-side can be derived by using the state equations in (1). Based on (13), the transition boundary with S_1 on is

$$\frac{L}{2C}(i_L - \frac{v_C}{R})^2 - (v_{in} - v_C)(v_C - v_{ref}) + \frac{L}{RC}(i_L - \frac{v_C}{R})(v_C - v_{ref}) = 0 \tag{14}$$

and the transition boundary with S_1 off is

$$\frac{L}{2C}(i_L - \frac{v_C}{R})^2 + v_C(v_C - v_{ref}) + \frac{L}{RC}(i_L - \frac{v_C}{R})(v_C - v_{ref}) = 0 \tag{15}$$

Detailed proofs of (14) and (15) are given in the Appendix.

Fig. 5 combines the transition boundaries of (14) and (15) together. Ideal σ^2 is close to σ^i and should be along the boundary between the reflective and refractive regions. However, k_1 and k_2 in (5) and (9), respectively, are taken to be constant values. These make the converter state possibly go through different operating regions before settling at the operating point. This phenomenon can be observed by considering the number of intersection points between σ^2 in (11) and the transition boundaries in (14) and (15).

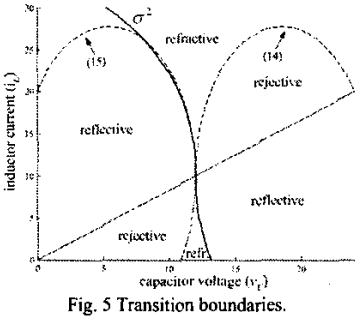

Fig. 5 Transition boundaries.

A. On-state trajectory

The intersection points of the on-state trajectory and the transition boundaries are determined by solving (11) and (14). Three possible solutions of $[i_{L,on}, v_{C,on}]$ are

$$[i^1_{L,on}, v^1_{C,on}] = [\frac{v_{ref}}{R}, v_{ref}] \tag{16}$$

$$[i^2_{L,on}, v^2_{C,on}] = [\frac{\alpha_1 L}{8C^2R^3k_1} - \frac{\alpha_1}{8CRk_1} + \frac{R}{2k_1}, \frac{\alpha_1 L}{8C^2R^2k_1}] \tag{17}$$

$$[i^3_{L,on}, v^3_{C,on}] = [\frac{\beta_1 L}{8C^2R^3k_1} - \frac{\beta_1}{8CRk_1} + \frac{R}{2k_1}, \frac{\beta_1 L}{8C^2R^2k_1}] \tag{18}$$

where $\alpha_1 = \Phi_1 + 4\sqrt{\Delta_1}$, $\beta_1 = \Phi_1 - 4\sqrt{\Delta_1}$, $\Phi_1 = -4(L - CR^2)$, and $\Delta_1 = L^2 - 2CLR^2 + 4C^2R^2k_1 v_{ref}$.

$[i^1_{L,on}, v^1_{C,on}]$ always occurs. $[i^2_{L,on}, v^2_{C,on}]$ will have real solutions for

$$\frac{1}{2}\cdot\frac{L}{Cv_{ref}} > k_1 \geq \frac{R^2}{4v_{ref}} \quad \text{, if } L - CR^2 \geq 0 \tag{19}$$

and

$$\frac{1}{2}\cdot\frac{L}{Cv_{ref}} > k_1 \geq \frac{2CLR^2 - L^2}{4C^2R^2v_{ref}} \quad \text{, if } L - CR^2 < 0 \tag{20}$$

$[i^3_{L,on}, v^3_{C,on}]$ will have real solutions for

having no real solution , if $L - CR^2 \geq 0$ (21)

and

$$\frac{R^2}{4v_{ref}} \geq k_1 > \frac{2CLR^2 - L^2}{4C^2R^2v_{ref}} \quad \text{, if } L - CR^2 < 0 \tag{22}$$

Derivations of (19)-(22) can be found in the Appendix. By combining (19)-(22), the value of k_1 that make the converter state go through the possible operating modes are tabulated in Table II.

B. Off-state trajectory

The intersection points of the on-state trajectory and the transition boundaries are determined by solving (11) and (15). Three possible solutions of $[i_{L,off}, v_{C,off}]$ are

$$[i^1_{L,off}, v^1_{C,off}] = [\frac{v_{ref}}{R}, v_{ref}] \tag{23}$$

$$[i^2_{L,off}, v^2_{C,off}] = [\frac{\alpha_2}{8C^2R^3k_2} - \frac{\alpha_2}{8CLRk_1} + \frac{CRv_{in}}{L} - \frac{R}{2k_2}, \frac{\alpha_2}{8C^2R^2k_2}] \tag{24}$$

$$[i^3_{L,off}, v^3_{C,off}] = [\frac{\beta_2}{8C^2R^3k_2} - \frac{\beta_2}{8CLRk_1} + \frac{CRv_{in}}{L} - \frac{R}{2k_2}, \frac{\beta_2}{8C^2R^2k_2}] \tag{25}$$

where $\alpha_2 = \Phi_2 - 4\sqrt{\Delta_2}$, $\beta_2 = \Phi_2 + 4\sqrt{\Delta_2}$,

$\Phi_2 = 8C^2R^2v_{in}k_2 + 4L^2 - 4CLR^2$, and

$\Delta_2 = L^4 - 2CL^3R^2 + 4C^2L^2R^2k_2(v_{in} - v_{ref})$.

$[i^1_{L,off}, v^1_{C,off}]$ always occurs. $[i^2_{L,off}, v^2_{C,off}]$ will have real solutions for

$$\frac{1}{2}\cdot\frac{L}{C(v_{in} - v_{ref})} > k_2 \geq \frac{R^2}{4(v_{in} - v_{ref})} \quad \text{, if } L - CR^2 \geq 0 \tag{26}$$

and

$$\frac{1}{2}\cdot\frac{L}{C(v_{in} - v_{ref})} > k_2 \geq \frac{2CLR^2 - L^2}{4C^2R^2(v_{in} - v_{ref})} \quad \text{, if } L - CR^2 < 0 \tag{27}$$

$[i^3_{L,off}, v^3_{C,off}]$ will have real solutions for

having no real solution, if $L - CR^2 \geq 0$ (28)

and

$$\frac{R^2}{4(v_{in}-v_{ref})} \geq k_2 > \frac{2CLR^2 - L^2}{4C^2R^2(v_{in}-v_{ref})}, \quad \text{if } L - CR^2 < 0 \quad (29)$$

Derivations of (26)-(29) can be found in the Appendix.

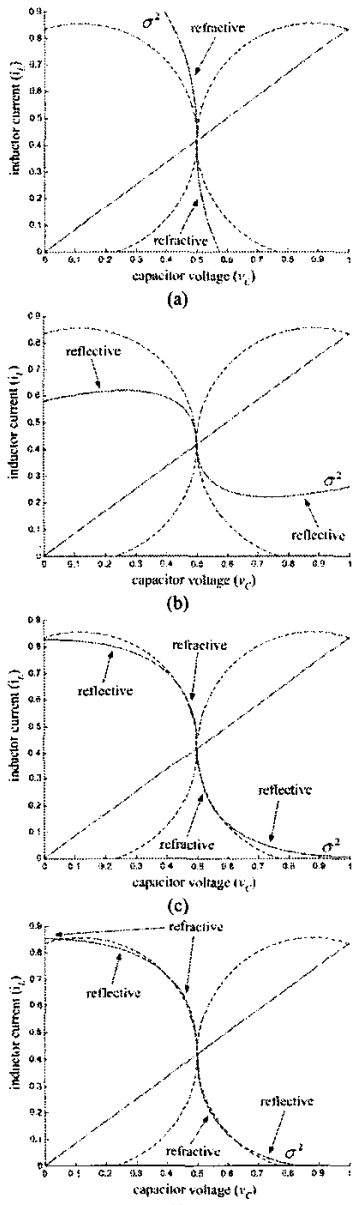

Fig. 6 Possible cases in the intersections between the switching surface and transition boundaries. [v_{in}=1, L=1, C=1, R=1.2, v_{ref}=0.5]. (a) Case I: Refractive region only with $\{k_1,k_2\}=\{0.326, 0.326\}$. (b) Case II: Reflective Region only with $\{k_1,k_2\}=\{1.5, 1.5\}$. (c) Case III: Along Two Regions with $\{k_1,k_2\}=\{0.731, 0.731\}$. (d) Case IV: Along Three Regions with $\{k_1,k_2\}=\{0.686, 0.686\}$.

By combining (26)-(29), the value of k_2 that make the converter state go through the possible operating modes are tabulated in Table II.

Fig. 6 depicts the situation of four possible cases, as described in Table II. Basically, when the state of the converter will move along the switching surface in the reflective region, which is similar to the sliding-mode control. Once the state enters into the boundary between the reflective and refractive regions, the system will go to the target operating point in the next switching action.

IV. EXPERIMENTAL VERIFICATIONS

A buck converter with the component values tabulated in Table I is studied. Fig. 7 shows the start-up trajectory, together with σ^1 and σ^2. σ^1 is formulated by having the same startup transients with σ^2 (i.e., σ^1 and σ^2 intercept at the points 'A' and 'B' in Fig. 7). The values of c_1 in (2), and k_1 in (11) can be shown to be equal to

$$c_1 = -\frac{v_{C,A} - v_{ref}}{i_{L,A} - \frac{v_{C,A}}{R}} \quad (30)$$

$$k_1 = -\frac{v_{C,A} - v_{ref}}{(i_{L,A} - \frac{v_{C,A}}{R})^2} \quad (31)$$

where $v_{C,A}$ and $i_{L,A}$ are the values of v_C and i_L at point 'A', respectively.

Detailed proof of (30) and (31) can be found in the Appendix.

k_2 in (11) is obtained by considering an arbitrary point (point 'C' in Fig. 7) on the state plane that

$$k_2 = -\frac{v_{C,C} - v_{ref}}{(i_{L,C} - \frac{v_{C,C}}{R})^2} \quad (32)$$

where $v_{C,C}$ and $i_{L,C}$ are the values of v_C and i_L at point 'C', respectively.

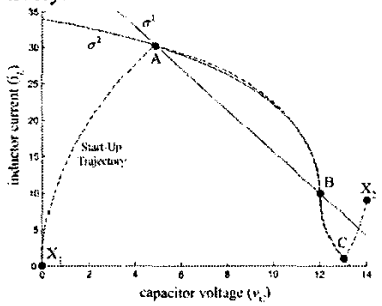

Fig. 7 Start-up transient response and the first and second-order switching surface. [Dotted line: start-up trajectory of buck converter]

Detailed proof of (32) can be found in the Appendix. The values of k_1 and k_2 that are chosen with this method gives a near optimum switching surface close to σ^i.

The hysteresis band in σ^1 is adjusted to give the same output ripple voltage at the rated power as with σ^2. Fig. 8 shows a comparison of the simulated transient responses when R is changed from 2.4Ω (60W) to 1.2Ω (120W), and

vice versa, with σ^1 and σ^2, respectively. The converter with σ^2 achieves faster transient response than that with σ^1. Fig. 9 shows the transient responses when R is changed from 2.4Ω (60W) to 24Ω (6W), in which the converter is operated in discontinuous conduction mode with R = 24Ω. Results show that steady state error exists with σ^1 and is zero with σ^2. The additional boundary due to the zero inductor current causes a shift of the effective output voltage reference. Figs. 10 and 11 show the experimental results corresponding to the above testing conditions and are in close agreement with the theoretical predictions. It can be observed that the converter can go to the steady state in two switching actions.

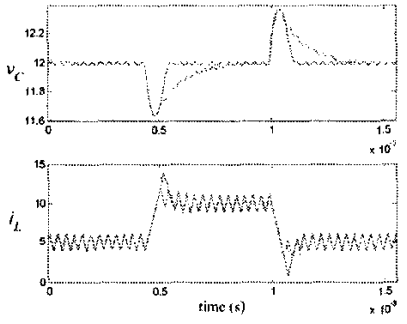

Fig. 8 Transient response of R from 2.4Ω to 1.2Ω and vice versus. [Solid line: σ^2, Dotted line: σ^1]

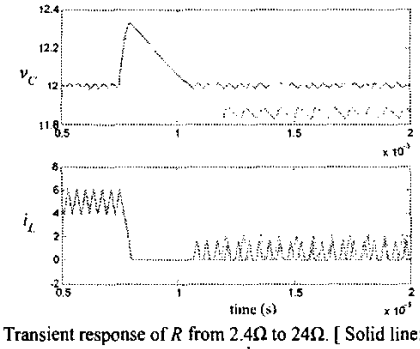

Fig. 9 Transient response of R from 2.4Ω to 24Ω. [Solid line: σ^2, Dotted line: σ^1]

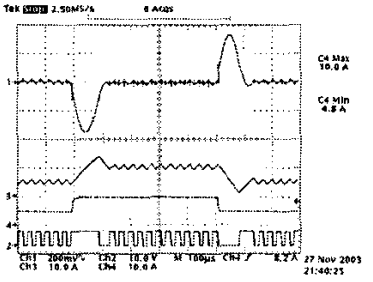

Fig. 10 Transient response of buck converter using second-order switching surface control. Load change from 5A(2.4Ω) to 10A(1.2Ω) and vice versus. [Ch1: v_c (200mV/div), Ch2: v_g(10V/div), Ch3: i_L(10A/div), Ch4: i_o(10A/div)] (Timebase: 100μs/div)

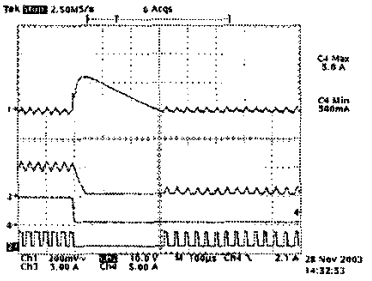

Fig. 11 Transient response of buck converter using second-order switching surface control. Load change from 5A(2.4Ω) to 0.5A(24Ω). [Ch1: v_c (200mV/div), Ch2: v_g(10V/div), Ch3: i_L(5A/div), Ch4: i_o(5A/div)] (Timebase: 100μs/div)

V. CONCLUSION

A boundary control using the second order switching surfaces in buck converter has been proposed. Large-signal stability and the transient response are investigated. Results show that second-order switching surface can achieve near-optimum large-signal responses and is also applicable for discontinuous conduction mode.

Table I Component values of the buck converter

Parameter	Value
v_{in}	24V
v_{ref}	12V
L	100μH
C	400μF
R	1.2 Ω
c_1	0.2702
$\{k_1, k_2\}$	{0.0104, 0.0104}

Table II: Number of intersection points between switching surface and transition boundary

			k_1 and off-state transition boundary		k_2 and on-state transition boundary	
Case	No. of inter-section	Operation Mode	If $L-CR^2<0$	If $L-CR^2\geq 0$	If $L-CR^2<0$	If $L-CR^2\geq 0$
I	1	Refractive Region only	$k_1 < \dfrac{2CR^2L-L^2}{4C^2R^2v_{ref}}$	$k_1 < \dfrac{R^2}{4v_{ref}}$	$k_2 < \dfrac{2CR^2L-L^2}{4C^2R^2(v_{in}-v_{ref})}$	$k_1 < \dfrac{R^2}{4(v_{in}-v_{ref})}$
II	1	Reflective Region only	$k_1 \geq \max\left\{\dfrac{L}{2Cv_{ref}}, \dfrac{R^2}{4v_{ref}}\right\}$	$k_1 \geq \dfrac{L}{2Cv_{ref}}$	$k_1 \geq \max\left\{\dfrac{L}{2C(v_{in}-v_{ref})}, \dfrac{R^2}{4(v_{in}-v_{ref})}\right\}$	$k_1 \geq \dfrac{L}{2C(v_{in}-v_{ref})}$
III	2	Pass Two Regions	$\max\left\{\dfrac{L}{2Cv_{ref}}, \dfrac{R^2}{4v_{ref}}\right\} > k_1 \geq \min\left\{\dfrac{L}{2Cv_{ref}}, \dfrac{R^2}{4v_{ref}}\right\}$	$\dfrac{L}{2Cv_{ref}} > k_1 \geq \dfrac{R^2}{4v_{ref}}$	$\max\left\{\dfrac{L}{2C(v_{in}-v_{ref})}, \dfrac{R^2}{4(v_{in}-v_{ref})}\right\} > k_1 \geq \min\left\{\dfrac{L}{2C(v_{in}-v_{ref})}, \dfrac{R^2}{4(v_{in}-v_{ref})}\right\}$	$\dfrac{L}{2C(v_{in}-v_{ref})} > k_2 \geq \dfrac{R^2}{4(v_{in}-v_{ref})}$
IV	3	Pass Three Regions	$\min\left\{\dfrac{L}{2Cv_{ref}}, \dfrac{R^2}{4v_{ref}}\right\} > k_1 \geq \dfrac{2CR^2L-L^2}{4C^2R^2v_{ref}}$	No solution	$\min\left\{\dfrac{L}{2C(v_{in}-v_{ref})}, \dfrac{R^2}{4(v_{in}-v_{ref})}\right\} > k_1 \geq \dfrac{2CR^2L-L^2}{4C^2R^2(v_{in}-v_{ref})}$	No solution

APPENDIX

1. *Proof of (13)*

By differentiating both sides of (12),

$$c_2 \frac{d(i_L - \frac{v_C}{R})^2}{dt} + \frac{d(v_C - v_{ref})}{dt} = 0$$

$$2 c_2 (i_L - \frac{v_C}{R})(\frac{di_L}{dt} - \frac{1}{R}\frac{dv_C}{dt}) + \frac{dv_C}{dt} = 0$$

$$\frac{\frac{di_L}{dt}}{\frac{dv_C}{dt}} = \frac{2 c_2 (i_L - \frac{v_C}{R})\frac{1}{R} - 1}{2 c_2 (i_L - \frac{v_C}{R})} \quad (A.1)$$

$$\frac{di_L}{dv_C} = \frac{1}{R} - \frac{1}{2 c_2 (i_L - \frac{v_C}{R})}$$

By equating $\sigma^2 = 0$ [Eq. (12)],

$$\frac{1}{c_2} = -\frac{(i_L - \frac{v_C}{R})^2}{v_C - v_{ref}} \quad (A.2)$$

Substitute it into (A.2) into (A.1), it can be shown that

$$\frac{di_L}{dv_C} = \frac{1}{R} + \frac{i_L - \frac{v_C}{R}}{2(v_C - v_{ref})} \quad (A.3)$$

2. *Proof of (14)*

When $q_1 = 1$ and $q_2 = 0$, Eq. (1) can be written as

$$\frac{di_L}{dt} = -\frac{1}{L} v_C + \frac{1}{L} v_{in} \quad (A.4)$$

$$\frac{dv_C}{dt} = \frac{1}{C} i_L - \frac{1}{RC} v_C \quad (A.5)$$

Based on (A.4) and (A.5),

$$\frac{\frac{di_L}{dt}}{\frac{dv_C}{dt}} = \frac{-\frac{1}{L} v_C + \frac{1}{L} v_{in}}{\frac{1}{C} i_L - \frac{1}{RC} v_C} \quad (A.6)$$

$$\left(\frac{di_L}{dv_C}\right)_{on} = \frac{C}{L}\left(\frac{v_{in} - v_C}{i_L - \frac{v_C}{R}}\right) \quad (A.7)$$

Compared (A.7) with (13), the transition boundary with S_1 on is

$$\frac{C}{L}\left(\frac{v_{in} - v_C}{i_L - \frac{v_C}{R}}\right) = \frac{1}{R} + \frac{1}{2}\frac{i_L - \frac{v_C}{R}}{v_C - v_{ref}} \quad (A.8)$$

It can be rewritten as

$$\frac{L}{2C}(i_L - \frac{v_C}{R})^2 - (v_{in} - v_C)(v_C - v_{ref}) + \frac{L}{RC}(i_L - \frac{v_C}{R})(v_C - v_{ref}) = 0 \quad (A.9)$$

3. *Proof of (15)*

When $q_1 = 0$ and $q_2 = 1$, Eq. (1) can be written as

$$\frac{di_L}{dt} = -\frac{1}{L} v_C \quad (A.10)$$

$$\frac{dv_C}{dt} = \frac{1}{C} i_L - \frac{1}{RC} v_C \quad (A.11)$$

Based on (A.10) and (A.11)

$$\frac{\frac{di_L}{dt}}{\frac{dv_C}{dt}} = \frac{-\frac{1}{L} v_C}{\frac{1}{C} i_L - \frac{1}{RC} v_C} \quad (A.12)$$

$$\left(\frac{di_L}{dv_C}\right)_{off} = -\frac{C}{L}\left(\frac{v_C}{i_L - \frac{v_C}{R}}\right) \quad (A.13)$$

Compared (A.13) with (13), the transition boundary with S_1 off is

$$-\frac{C}{L}\left(\frac{v_C}{i_L - \frac{v_C}{R}}\right) = \frac{1}{R} + \frac{1}{2}\frac{i_L - \frac{v_C}{R}}{v_C - v_{ref}} \quad (A.14)$$

It can be rewritten as

$$\frac{L}{2C}(i_L - \frac{v_C}{R})^2 + v_C(v_C - v_{ref}) + \frac{L}{RC}(i_L - \frac{v_C}{R})(v_C - v_{ref}) = 0 \quad (A.15)$$

4. *Proof of (19)-(22)*

The solutions are real if

$$\Delta_1 \geq 0 \quad \Rightarrow \quad k_1 \geq \frac{2CLR^2 - L^2}{4C^2R^2 v_{ref}} \quad (A.16)$$

They must also satisfy the conditions of

$$v_{C,on} \geq 0 \quad (A.17)$$

and

$$i_{L,on} - \frac{v_{C,on}}{R} > 0 \quad (A.18)$$

Thus, by considering (16)-(18), and (A.17),

$$\alpha_1 \geq 0 \quad \Rightarrow \quad \Phi_1 + 4\sqrt{\Delta_1} \geq 0 \quad (A.19)$$

and

$$\beta_1 \geq 0 \quad \Rightarrow \quad \Phi_1 - 4\sqrt{\Delta_1} \geq 0 \quad (A.20)$$

Based on (A.19), it can be shown that

$$k_1 \geq \frac{2CLR^2 - L^2}{4C^2R^2 v_{ref}} \quad \text{if } L - CR^2 < 0 \quad (A.21)$$

and

$$k_1 \geq \frac{R^2}{4v_{ref}} \quad \text{if } L - CR^2 \geq 0 \quad (A.22)$$

will give real solutions.

Based on (A.20), it can be shown

$$k_1 \leq \frac{R^2}{4 v_{ref}} \quad \text{if } L - CR^2 < 0 \quad (A.23)$$

will have a real solution. There is no real solution for $L - CR^2 \geq 0$.

By substituting the solution set of (17) into (A.18), it can be shown that

$$k_1 < \frac{1}{2} \cdot \frac{L}{C v_{ref}} \quad (A.24)$$

will have a real solution.

Similarly, by substituting the solution set of (18) into (A.18),

$$k_1 > \frac{2CLR^2 - L^2}{4C^2R^2 v_{ref}} \quad (A.25)$$

will have a real solution.

Thus, based on (A.16), (A.21), (A.22) and (A.24), (19) and (20) can be obtained. Based on (A.16), (A.23) and (A.25), (21) and (22) can be obtained.

5. Proof of (26)-(29)

The solutions are real if

$$\Delta_2 \geq 0 \quad \Rightarrow \quad k_2 \geq \frac{2CLR^2 - L^2}{4C^2R^2(v_{in} - v_{ref})} \tag{A.26}$$

They must also satisfy the conditions of

$$v_{C,off} \leq v_{in} \tag{A.27}$$

and

$$i_{L,off} - \frac{v_{C,off}}{R} < 0 \tag{A.28}$$

Thus, based on (23)-(25), and (A.27),

$$\alpha_2 - 8C^2R^2 v_{in} k_2 \leq 0 \tag{A.29}$$

and

$$\beta_2 - 8C^2R^2 v_{in} k_2 \leq 0 \tag{A.30}$$

By using (A.29), it can be shown that

$$k_2 \geq \frac{2CLR^2 - L^2}{4C^2R^2(v_{in} - v_{ref})}, \quad \text{if } L - CR^2 < 0 \tag{A.31}$$

and

$$k_2 \geq \frac{R^2}{4(v_{in} - v_{ref})}, \quad \text{if } L - CR^2 \geq 0 \tag{A.32}$$

will give real solutions.

Based on (A.30), it can be shown that

$$k_2 \leq \frac{R^2}{4(v_{in} - v_{ref})}, \quad \text{if } L - CR^2 < 0 \tag{A.33}$$

will have a real solution. There is no real solution for $L - CR^2 \geq 0$.

By substituting the solution set of (24) into (A.28), it can be shown that

$$k_2 < \frac{1}{2} \cdot \frac{L}{C(v_{in} - v_{ref})} \tag{A.34}$$

will give a real solution.

By substituting the solution set of (25) into (A.28), it can be shown that

$$k_2 > \frac{2CLR^2 - L^2}{4C^2R^2(v_{in} - v_{ref})} \tag{A.35}$$

will give a real solution.

Thus, based on (A.26), (A.31), (A.32) and (A.34), (26) and (27) can be obtained. Based on (A.26), (A.33) and (A.35), (28) and (29) can be obtained. The above calculation for k_2 is valid for $i^2_{L,off} > 0$ and $i^3_{L,off} > 0$.

6. Proof of (30)-(31)

The start-up on-state trajectory (i.e., 'X_1' to 'A' in Fig. 7) can be written as

$$\dot{x} = (A_0 + A_1)x + (B_0 + B_1)u, \quad x_0 = x_{X_1} \tag{A.36}$$

The off-state trajectory (i.e., 'A' to 'B' in Fig. 7) can be replaced with the equivalent time reversed system given by

$$\dot{x} = -(A_0 + A_2)x - (B_0 + B_2)u, \quad x_0 = x_B \tag{A.37}$$

where multiplying the system's A and B matrices by -1 reverses the state velocity vector and therefore gives the output $x(-t)$.

The intersection point 'A' of vector $x_A = [i_{L,A} \quad v_{C,A}]$ can be obtained by solving (A.36) and (A.37) numerically. By substituting $v_{C,A}$ and $i_{L,A}$ into (2), it can be shown that

$$c_1 = -\frac{v_{C,A} - v_{ref}}{i_{L,A} - \frac{v_{C,A}}{R}} \tag{A.38}$$

By substituting $v_{C,A}$ and $i_{L,A}$ into (12), it can be shown that

$$k_1 = -\frac{v_{C,A} - v_{ref}}{(i_{L,A} - \frac{v_{C,A}}{R})^2} \tag{A.39}$$

7. Proof of (32)

The off-state trajectory (i.e., 'X_2' to 'C' in Fig. 7) can be written as

$$\dot{x} = (A_0 + A_2)x + (B_0 + B_2)u, \quad x_0 = x_{X_2} \tag{A.40}$$

The on-state trajectory (i.e., from point 'C' to point 'B' in Fig. 7) can be replaced with the equivalent time reversed system given by

$$\dot{x} = -(A_0 + A_1)x - (B_0 + B_1)u, \quad x_0 = x_B \tag{A.41}$$

The intersection point 'C' of vector $x_C = [i_{L,C} \quad v_{C,C}]$ can be obtained by solving (A.40) and (A.41) numerically. By substituting $v_{C,C}$ and $i_{L,C}$ into (12), it can be shown that

$$k_2 = \frac{v_{C,C} - v_{ref}}{(i_{L,C} - \frac{v_{C,C}}{R})^2} \tag{A.42}$$

REFERENCES

[1] P.T. Krein, "Chapter 8: Nonlinear Control and Control of Chaos," *Nonlinear Phenomena in Power Electronics: Attractors, Bifurcation, Chaos, and Nonlinear Control*, IEEE Press, 2001.

[2] R. Munzert and P.T. Krein, "Issues in Boundary Control," *in Proc. IEEE Power Electron. Spec. Conf.*, pp. 810-816, 1996.

[3] M. Greuel, R. Muyshondt and P.T. Krein, "Design Approaches to Boundary Controllers" *in Proc. IEEE Power Electron. Spec. Conf.*, pp. 672-678, 1997.

[4] M. Carpita and M. Marchesoni, "Experimental Study of a Power Conditioning System using Sliding Mode Control," *IEEE Trans. Power Electron.*, vol. 11, no. 5, pp. 731-742, Sept. 1996.

[5] B. J. Cardoso, A. F. Moreira, B.R. Menezes and P.C. Cortizo, "Analysis of Switching Frequency Reduction Methods Applied to Sliding-Mode Controlled DC-DC Converters," in *Proc. IEEE Power Electron. Spec. Conf.*, pp. 672-678, 1992.

[6] C. H. Tso and J. C. Wu, "A Ripple Control Buck Regulator with Fixed Output Frequency," *IEEE Power Electronics Letter*, vol. 1, no. 3, pp. 61-63, Sept. 2003.

[7] R. Miftakhutdinov, "Analysis of Synchronous Buck Converter with Hysteretic Controller at High Slew-Rate Load Current Transients," in *Proc. High Frequency Power Conversion Conference*, 1999, pp. 55-69, 1999.

[8] V.M. Nguyen and C.Q. Lee, "Tracking Control of Buck Converter using Sliding-Mode with Adaptive Hysteresis," *in Proc. IEEE Power Electronics Specialists Conference*, pp. 1086-1093, 1995.

[9] A. Kislovski, R. Redl, and N. Sokal, "Dynamic Analysis of Switching-Mode DC-DC converters," Van Nostrand Reinhold, 1991.